



Temperature dependence of the emission cross-section and fluorescence lifetime in Cr:LiCAF, Cr:LiSAF, and Cr:LiSGaF between 78 K and 618 K

SERDAR OKUYUCU,^{1,2,3,*}  JELTO THESINGA,¹ HIROKI TANAKA,⁴ 
YUSUF OZTURK,²  FRANZ X. KÄRTNER,^{1,5,6}  MIKHAIL
PERGAMENT,¹  AND UMIT DEMIRBAS^{1,2} 

¹Center for Free-Electron Laser Science CFEL, Deutsches Elektronen-Synchrotron DESY, Notkestr. 85, 22607 Hamburg, Germany

²Laser Technology Laboratory, Department of Electrical and Electronics Engineering, Antalya Bilim University, 07190, Antalya, Turkey

³Akdeniz University, Department of Electrical-Electronics Engineering, Antalya, Turkey

⁴Leibniz-Institut für Kristallzüchtung (IKZ), Max-Born-Straße 2, 12489 Berlin, Germany

⁵Physics Department, University of Hamburg, Luruper Chaussee 149, 22761 Hamburg, Germany

⁶The Hamburg Centre for Ultrafast Imaging, Luruper Chaussee 149, 22761 Hamburg, Germany

*serdar.okuyucu@desy.de

Abstract: Cr:Colquiriites (Cr:LiCAF, Cr:LiSAF, and Cr:LiSGaF) are well-known for their broad emission bands in the near-infrared region. Unfortunately, due to their relatively weak thermomechanical strength, average powers from Cr:Colquiriite lasers have been so far limited to sub-5 W level in continuous-wave operation at room temperature. In this study, the promise of cryogenic operation, which shows significant power scalability in Yb-based systems, is investigated in detail for Cr-doped Colquiriite crystals in terms of the temperature dependence of the fluorescence lifetime and emission cross-section (σ_e) in the 78–618 K range. The lifetime measurements showed that the fluorescence, as well as the radiative lifetimes of Cr:Colquiriites are temperature dependent. The emission cross-section measurements revealed that while cooling the crystals from 300 K to 78 K, the peak σ_e in E||c polarization increases moderately for all crystals: from around $1.3 \times 10^{-20} \text{ cm}^2$ to $1.6 \times 10^{-20} \text{ cm}^2$ in Cr:LiCAF, from around $4.5 \times 10^{-20} \text{ cm}^2$ to $6.3 \times 10^{-20} \text{ cm}^2$ in Cr:LiSAF and from around $3.1 \times 10^{-20} \text{ cm}^2$ to $3.95 \times 10^{-20} \text{ cm}^2$ in Cr:LiSGaF. We provide analytical formulas describing the measured temperature dependence of all relevant quantities such as fluorescence/radiative lifetime, peak emission wavelength, peak emission cross-section, and emission full-width at half-maximum. Overall, the reported results constitute a solid basis for the modeling of Cr:Colquiriite-based laser and amplifier systems, especially for the assessment of their potential at cryogenic temperatures.

Published by Optica Publishing Group under the terms of the [Creative Commons Attribution 4.0 License](https://creativecommons.org/licenses/by/4.0/). Further distribution of this work must maintain attribution to the author(s) and the published article's title, journal citation, and DOI.

1. Introduction

Chromium (Cr) is among the most widely utilized laser-active dopants [1], and its different charge states provide broadband vibronic lasing in various spectral regions (Cr²⁺, Cr³⁺, and Cr⁴⁺ based solid-state lasers cover the approximate tuning ranges of 1850–3350 nm [2,3], 700–1100 nm [4], and 1100–1600 nm [5], respectively). Among these charge states of chromium, Cr³⁺ is one of the most popular states, which was also employed as the optical gain material in the first experimental demonstration of lasing action in ruby (Cr³⁺:Al₂O₃) [6]. In the past decades, laser action of Cr³⁺ has been achieved in many other hosts such as garnets, silicates,

tungstates, borates, and niobates [7]. Unfortunately, for most of these hosts, achievable laser efficiencies are rather low due to (i) difficulty in growing large-size high-quality crystals and (ii) the existence of strong excited-state absorption (ESA) [7]. So far, efficient lasing has been demonstrated in $\text{Cr}^{3+}:\text{Be}_3\text{Al}_2(\text{SiO}_3)_6$ (emerald) [8,9], $\text{Cr}^{3+}:\text{BeAl}_2\text{O}_4$ (alexandrite) [10,11], and Cr^{3+} doped Colquiriites such as $\text{Cr}:\text{LiCaAlF}_6$ ($\text{Cr}:\text{LiCAF}$) [12,13], $\text{Cr}:\text{LiSrAlF}_6$ ($\text{Cr}:\text{LiSAF}$) [7] and $\text{Cr}:\text{LiSrGaAlF}_6$ ($\text{Cr}:\text{LiSGAF}$) [14].

The physical structure of the host material influences/perturbs the dopant ion, and this leads to different sets of optical properties (i.e., energy levels, absorption, stimulated cross-section, radiative and non-radiative lifetimes, and transition linewidth) in each host. The nature of the emission linewidths in different hosts of Cr^{3+} is determined by the strength of the crystal field which is categorized as strong, moderate, and weak [15]. Ruby is an example of a high-crystal-field material, where a strong narrow-line emission at 694.3 nm dominates lasing (from ${}^2\text{E}$ to ${}^4\text{A}_2$ transition) [6]. In alexandrite, a moderate crystal field exists, which allows both narrow-line (from ${}^2\text{E}$ to ${}^4\text{A}_2$ transition) and broadband (from ${}^4\text{T}_2$ to ${}^4\text{A}_2$) lasing emission [16]. In $\text{Cr}^{3+}:\text{Colquiriites}$, a low-intensity crystal field exists that induces broad emission linewidths via the phonon-broadened ${}^4\text{T}_2$ to ${}^4\text{A}_2$ transition, resulting in a widely tunable laser operation in the near-infrared region between 700 and 1100 nm [1,4,15,17,18]. The broad gain bandwidths in $\text{Cr}^{3+}:\text{Colquiriites}$ enable the generation of sub-10-fs level pulses in mode-locked regime [19–22], making them a strong competitor to $\text{Ti}:\text{Sapphire}$ laser systems [23]. $\text{Cr}:\text{Colquiriites}$ can be directly diode-pumped by commercially available low-cost AlGaInP diode lasers around 670 nm, enabling the construction of compact and robust laser systems. Moreover, they can be grown with very low passive losses below 0.2% per cm [24], and hence one can build high-Q cavities with ultralow lasing threshold [25], and use the stored intracavity energy levels for achieving oscillators with attosecond level timing jitter noise [26].

On the other hand, power scaling efforts with $\text{Cr}:\text{Colquiriites}$ have been quite challenging owing to their relatively poor thermomechanical properties along with the presence of several undesired thermal loading mechanisms such as thermal quenching, ESA, and Auger upconversion [4, 27–31]. As an example, the thermal conductivity of $\text{Cr}:\text{LiSAF}$ is an order of magnitude lower than that of $\text{Ti}:\text{Sapphire}$, and is only a quarter of the value of $\text{Yb}:\text{YAG}$ [4]. As a result, despite their moderate quantum defect levels (15–25%), their low thermal conductivity results in relatively rapid heating of the $\text{Cr}:\text{Colquiriite}$ crystals, which then induces additional heating mechanisms via temperature quenching of fluorescence lifetime. On the positive side, thermal lensing in $\text{Cr}:\text{Colquiriites}$ is rather weak since the thermal lensing caused by the temperature-dependent refractive index is compensated by the opposite lensing effect induced by the photoelastic stress inside the crystals [32]. Overall, the achievable continuous-wave laser power levels from $\text{Cr}:\text{Colquiriites}$ have been so far limited to 3 W in $\text{Cr}:\text{LiSAF}$ [33–35], 2.5 W in $\text{Cr}:\text{LiCAF}$ [36], and 1.2 W in $\text{Cr}:\text{LiSGaF}$ [14]. Higher average power levels are so far only attained in pulsed operation at very low repetition rates (2 J pulses at 15 Hz [37], 8.8 J pulses at 5 Hz [38]).

Cryogenic operation of solid-state lasers has been shown to provide great power scalability for various gain media including $\text{Yb}:\text{YAG}$ [39,40], $\text{Yb}:\text{YLF}$ [41,42], $\text{Nd}:\text{YAG}$ [43], and $\text{Ti}:\text{Sapphire}$ [44]. The performance improvement at reduced temperatures is due to the improvement in spectroscopic, mechanical, and thermo-optic properties [45]. For example, in the case of $\text{Yb}:\text{YAG}$ ($\text{Ti}:\text{Sapphire}$), the thermal conductivity improves 4-fold (30-fold), the thermal expansion coefficient reduces 3-fold (15-fold), the thermo-optic coefficient reduces 8-fold (7-fold) [44], and the emission cross-section improves 5-fold (not reported yet for $\text{Ti}:\text{Sapphire}$) when cooled from 300 K to 100 K [41], enabling the construction of higher-power laser/amplifier systems with better beam quality in cryogenic operation. Despite the demonstrated performance of $\text{Cr}:\text{Colquiriites}$ at room temperature, to our knowledge, almost no effort has been made for the investigation of their spectroscopic and thermo-opto-mechanical properties at cryogenic temperatures [4]. Hence, as a starting point, a detailed temperature-dependent characterization of spectroscopic properties in

Cr:Colquiriites is then of significant importance for the efficient use and accurate modeling of laser and amplifier systems pumped with high-power red-diode sources and exploration of their potential at cryogenic temperatures.

In this work, we have investigated the temperature dependence of fluorescence lifetime and emission cross-section in Cr:LiCAF, Cr:LiSAF, and Cr:LiSGaF crystals at cryogenic (78-300 K) and at elevated temperatures up to 618 K. Fluorescence lifetime measurements indicated that the quantum efficiency of the crystals stays above 90% up to 510 K in Cr:LiCAF, 315 K in Cr:LiSAF, and 325 K in Cr:LiSGaF, respectively. A limited improvement in emission strength in E||c polarization is obtained while going to cryogenic temperatures: ~1.2-fold in Cr:LiCAF, ~1.4-fold in Cr:LiSAF, and ~1.3-fold in Cr:LiSGaF. The emission width at 80 K is found to be still as broad as 100 nm, 140 nm, and 125 nm for the case of Cr:LiCAF, Cr:LiSAF, and Cr:LiSGaF, respectively. Empirical formulas reporting the temperature dependence of all relevant spectroscopic quantities are presented. To our knowledge, this work stands as the first study reporting temperature dependence of fluorescence lifetime and emission cross section in Cr:Colquiriite crystals in detail. The reported results may aid laser engineers and scientists in designing room-temperature and cryogenic Cr:Colquiriite-based laser and amplifier systems.

The paper is organized as follows: Section 2 describes the experimental setups used in the temperature-dependent characterization of fluorescence lifetime and emission cross-section (in E⊥c and E||c) for Cr:Colquiriites. In section 3, we present the results of experimental findings for each Cr:Colquiriite crystal and discuss the results. A short conclusion and outlook for future work are provided in Section 4.

2. Experimental methodology

2.1. Fluorescence lifetime measurements

Figures 1 (a) and (b) show the experimental setups used for the measurement of temperature-dependent fluorescence lifetime in Cr:Colquiriites over 78-300 K and 300-618 K ranges, respectively. In both setups, a 1.8 W multi-mode laser diode (MMD) with a narrow emission peak at 657 nm is used as the excitation source. The MMD output is first collimated with an aspheric lens ($f_1 = 4.5$ mm), and then an achromatic doublet with $f_2 = 100$ mm is used to loosely focus the pump beam into the crystal (tight focusing is not applied to prevent lifetime quenching via the Auger upconversion process). Even though the overlap between the absorption and emission bands of the crystals under investigation is rather small, the crystals are excited from their edge to further minimize radiation trapping [4]. The pump beam is then modulated using a delay generator (DG in Fig. 1) to produce 1 ms long rectangular excitation pulses, with sharp (sub-microsecond) rising and falling edges, at a repetition rate of 10 Hz (average power incident on crystals: 180 mW). The emitted fluorescence is collected by an uncoated lens ($f_3 = 50$ mm) and is detected using a photodetector placed at 90° in the direction of the excitation beam.

In the experiments, the following a-cut Cr:Colquiriite crystals grown at the Institute for Crystal Growth (IKZ) in Berlin were utilized: (i) a rod-shaped Cr:LiCAF crystal with a length of 16.7 mm, a diameter of 4.7 mm, and Cr-doping level of 3 mol%, (ii) a 15 mm long, 2 mm thick Brewster-Brewster cut Cr:LiSAF slab sample with a thickness of 2 mm and doping of 0.8 mol%, (iii) a cuboid-shaped Cr:LiSGaF crystal with a length of 1.5 mm, aperture of 6×5 mm² and Cr-doping level of 3 mol%. For the 3 mol% (LiCAF, LiSGaF) and 0.8 mol% (LiSAF) Cr-doped Colquiriites under investigation, the concentration quenching of fluorescence lifetime is negligible according to the literature (for 2-15 mol% Cr-doping in LiSAF [46], for 0.3-8.8 mol% Cr-doping in LiCAF [13,47,48]).

In experiments performed at cryogenic temperatures (78-300 K, Fig. 1 (a)), the Cr:Colquiriite samples are mounted on copper holders of suitable geometry for each respective sample. A firm physical and thermal contact between crystals and respective holders is maintained by the use of thin indium sheets. The crystal holder is in turn firmly fixed on the top of a multi-stage cold head

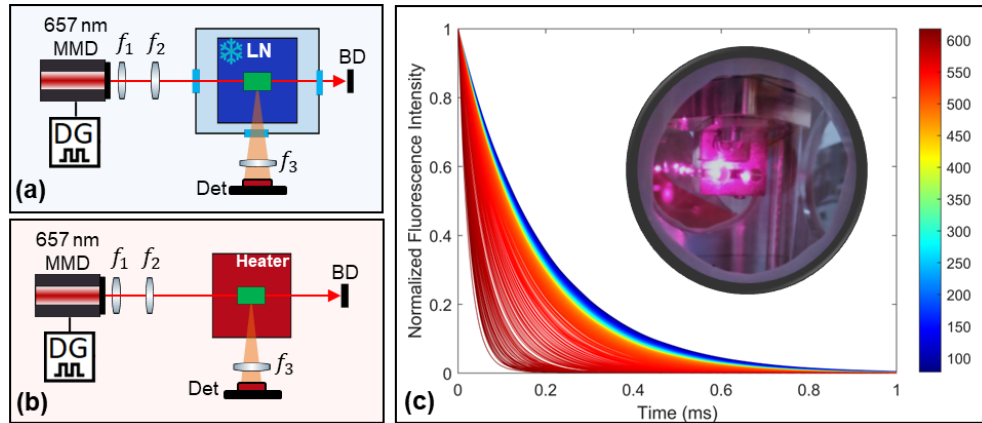


Fig. 1. Simplified schematic of the temperature-dependent fluorescence lifetime measurement setups used for (a) 78 - 300 K and (b) 300 - 618 K ranges. (c) Fluorescence decay curves of Cr:LiCAF measured at 1 K increments over the 78-618 K range (temperature color map is shown on the right in K). The inset shows the Cr:LiCAF crystal inside the dewar.

inside a vacuum-sealed dewar. The dewar tank is filled with liquid nitrogen for cooling crystals down to 78 K. The temperature-dependent fluorescence lifetime is then measured during the slow heating cycle of the dewar (heating from 78 to 300 K took around 4 hours). A temperature sensor attached to the crystal holder enabled real-time measurement of crystal temperature with ± 0.1 K accuracy. In experiments performed at above room temperature (>300 K, Fig. 1 (b)), the Cr:Colquiriite crystals in respective holders are placed directly on top of a heating plate that enabled controlling the temperature of crystals up to 618 K.

By use of the setups shown in Figs. 1 (a,b), the fluorescence decay for each Cr:Colquiriite crystal is collected at 1 K increments over their respective temperature range (78-618 K for Cr:LiCAF, 78-478 K for Cr:LiSAF, 78-471 K for Cr:LiSGaF). A small-area (0.8 mm^2) 350 MHz free-space Si detector (Thorlabs DET10A2) was used in the experiments. The Si detector has 1 ns rise time for 50-ohm termination, and sub-25 ns response time could be achieved while using a 1k-ohm termination. As an example, the fluorescence decay curves of Cr:LiCAF measured in the 78-618 K range are shown in Fig. 1 (c). A single exponential decay model provided a very good fit to the measured data at all temperatures for all Cr:Colquiriite crystals under investigation. The estimated error bar in lifetime measurements is around $\pm 0.25 \text{ } \mu\text{s}$ at room temperature and below and is around $\pm 0.75 \text{ } \mu\text{s}$ at elevated temperatures. The resulting measurements of the temperature-dependent fluorescence lifetime for Cr:Colquiriites are discussed further in Section 3. Here, we limit the upper temperature applied in the case of Cr:LiSAF and Cr:LiSGaF to around 480 K, since above this temperature, these crystals mostly decay nonradiatively so the radiative emission signal almost disappears.

2.2. Emission cross-section measurements

The experimental setups used for the determination of temperature-dependent σ_e in $E \perp c$ and $E \parallel c$ polarizations of Cr:LiCAF, Cr:LiSAF, and Cr:LiSGaF crystals are shown in Fig. 2. A $\sim 250 \text{ mW}$ continuous-wave output (at 660 nm) from a single-mode diode (SMD) is used for the excitation of crystals. For Cr:LiCAF and Cr:LiSGaF, the emission intensity spectra are measured at a 90° angle to the pump propagation direction. For Cr:LiSAF, due to the Brewster cut geometry of the crystal at hand, the emission intensity spectra are measured in the transmitted pump beam direction to capture the emission intensity in both $E \perp c$ and $E \parallel c$ polarizations (shown in Fig. 2 (c,d)). A small aperture beam dump placed at the exit blocked the transmitted pump beam.

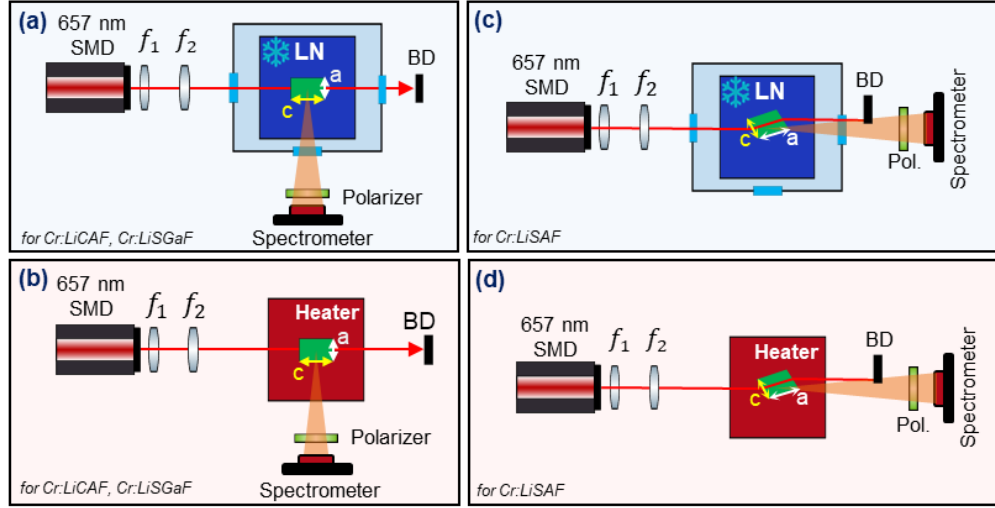


Fig. 2. Simplified schematic of the temperature-dependent σ_e measurement setups used for (a-b) Cr:LiCAF & Cr:LiSGaF and (c-d) Cr:LiSAF. Setups (a-c) and (b-d) are for cryogenic and room/elevated temperature experiments, respectively.

In all measurements, a linear thin film polarizer (Thorlabs LPNIRE100-B) with an extinction ratio above 400:1 is used for selecting the fluorescence emission in the relevant polarizations. The respective fluorescence in each polarization is then collected by an uncoated plano-convex lens (Newport KPX076) with a focal length of 25.4 mm and fed into the Yokogawa AQ6315A optical spectrum analyzer via a 400 μm core size fiber (internal spectral resolution setting: 1 nm, effective resolution of the device: 2 nm). At each temperature, 1000 data points are recorded within the spectral range of 600–1400 nm, at an average wavelength separation of ~ 0.8 nm. The spectral resolution setting is adequate as we have confirmed that, Cr:Colquiriites do not possess any closely-spaced sharp emission lines within the temperature range of interest. For improving SNR, at each temperature, the average of 64 measurements is recorded as the intensity spectrum in each polarization.

The emission cross-section in absolute units for $E \perp c$ ($\sigma_{e,a}$) and $E \parallel c$ ($\sigma_{e,c}$) polarizations are then calculated using the modified Füchtbauer–Ladensburg formula [49–51]

$$\sigma_{e,a}(\lambda, T) = \frac{\lambda^5}{8\pi cn^2 \tau_R(T)} \frac{I_a(\lambda)}{\int \left(\frac{1}{3} I_c(\lambda) + \frac{2}{3} I_a(\lambda) \right) \lambda d\lambda} \quad (1)$$

$$\sigma_{e,c}(\lambda, T) = \frac{\lambda^5}{8\pi cn^2 \tau_R(T)} \frac{I_c(\lambda)}{\int \left(\frac{1}{3} I_c(\lambda) + \frac{2}{3} I_a(\lambda) \right) \lambda d\lambda} \quad (2)$$

where $I_{a,c}(\lambda)$ are the measured emission intensities in the $E \perp c$ and $E \parallel c$ polarizations of the uniaxial crystal, c is the speed of light in vacuum, λ is wavelength, n is the average refractive index of the gain medium ($n = 1.41$ for Cr:Colquiriites), and $\tau_R(T)$ is the radiative lifetime of the upper laser level. The nature of temperature dependence of $\tau_R(T)$ is modeled (Eq. (3)) from measurements of fluorescence lifetime performed in this work and is discussed in section 3.1.

As an example, the measured σ_e spectra of Cr:LiCAF in the 78–618 K range are illustrated in Fig. 3. Within expectations, the increased temperature causes a red-shift of the emission wavelength, and the full-width at half maximum (FWHM) of the emission increases with temperature. On the other hand, the peak emission strength in $E \parallel c$ polarization increases whereas

interestingly a slight decrease is observed in $E_{\perp c}$ polarization when the crystal is cooled to cryogenic temperatures. For all three Cr:Colquiriite crystals under investigation, a detailed quantitative characterization of temperature-dependent emission cross-section in terms of peak σ_e strength, FWHM, and peak σ_e wavelength in $E_{\parallel c}$ and $E_{\perp c}$ polarizations will be given in section 3.2.

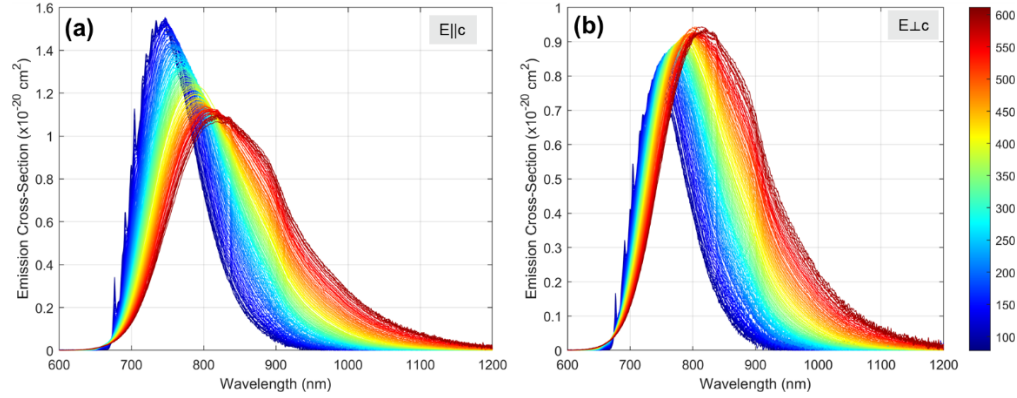


Fig. 3. Measured variation of σ_e with temperature for Cr:LiCAF in the 78-618 K range for (a) $E_{\parallel c}$ and (b) $E_{\perp c}$ polarizations. Temperature color map is shown on the right in K

3. Results and discussion

3.1. Fluorescence lifetime measurement results

The temperature dependence of the fluorescence lifetime for the three Cr:Colquiriite crystals are summarized in Fig. 4. In this figure, the red symbols represent the experimentally measured fluorescence lifetime data (as the data is taken with 1 K intervals, the points look like a line). The solid and dashed curves in Fig. 4 are numerical fits to the data that we will outline shortly.

First of all, as we can see from the graphs, there are two clear distinct trends in the measured fluorescence lifetime data: (i) a slow quasi-linear variation in the low-temperature regime, and (ii) a sharp sudden decrease at elevated temperatures. At low temperatures (below ~ 300 K), the nonradiative decay rate is ignorable in Cr:Colquiriites, and the observed temperature dependence is mostly determined by the temperature variation of the radiative lifetime $\tau_R(T)$. In this low-temperature regime, as proposed by Andrews *et al.*, one can use the following empirical formula to fit the measured variation of lifetime [52]:

$$\frac{1}{\tau_R(T)} = \frac{1}{\tau_{R0}} e^{\alpha T}. \quad (3)$$

In Eq. (3), τ_{R0} is the low temperature limit of radiative lifetime and α is an empirical fit coefficient.

The significantly reduced lifetimes measured at elevated temperatures (above 400 K) are due to the nonradiative process and are also referred to as thermal quenching of fluorescence lifetime. At elevated temperatures, the nonradiative lifetime $\tau_{NR}(T)$ starts to decrease and become dominant in determining the temperature dependence of measured fluorescence lifetime. This process can be described by a single configurational coordinate Mott model [52,53] as follows:

$$\frac{1}{\tau_{NR}(T)} = \frac{1}{\tau_{NR0}} e^{\left(-\frac{\Delta E}{kT}\right)}, \quad (4)$$

where τ_{NR0} is the high-temperature limit of the nonradiative lifetime, k is the Boltzmann constant, and ΔE is the activation energy (energy gap between the minimum of the 4T_2 excited state and

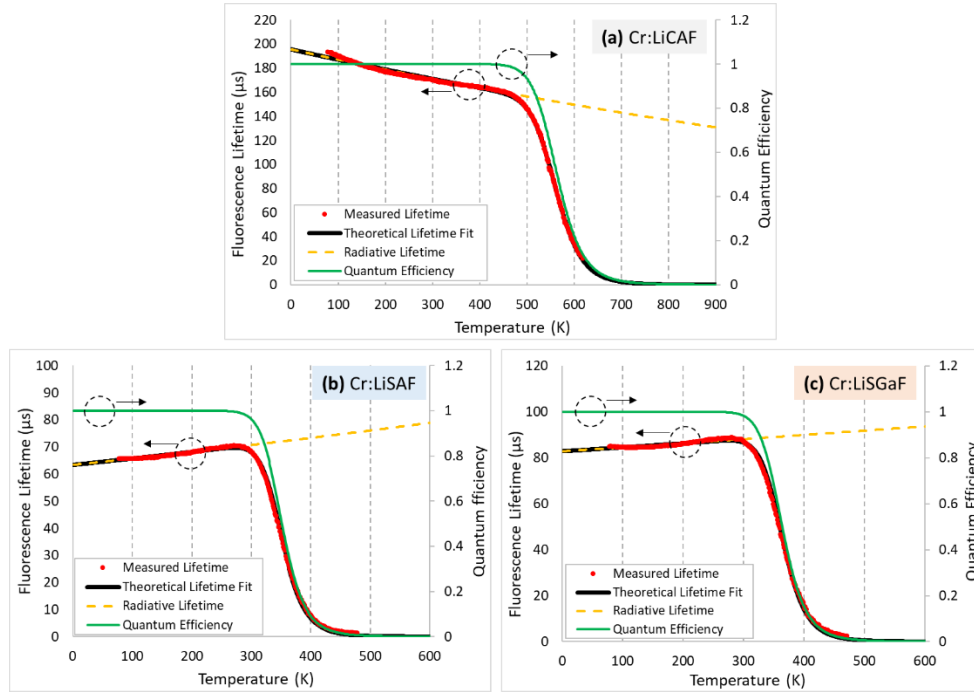


Fig. 4. Measured dependence of fluorescence lifetime on temperature for (a) Cr:LiCAF, (b) Cr:LiSAF, and (c) Cr:LiSGaF. The red symbols indicate the experimentally measured data, whereas the black lines are analytical fits to the measured data using the Mott model. The goodness of the fit to the measured lifetime is quantified by the R-square test ($R^2 = 0.9989$ for Cr:LiCAF, $R^2 = 0.9998$ for Cr:LiCAF, and Cr:LiSGaF). The analytical estimates for the radiative lifetime are represented by gold color dashed lines and the quantum efficiency is plotted as solid green lines.

the crossing point of 4T_2 excited state with the 4A_2 ground state [54]). Then, the overall variation of measured fluorescence lifetime with temperature $\tau_F(T)$ could be described as the combined rate of radiative and nonradiative transitions as follows:

$$\frac{1}{\tau_F(T)} = \frac{1}{\tau_R(T)} + \frac{1}{\tau_{NR}(T)} = \frac{1}{\tau_{R0}} e^{\alpha T} + \frac{1}{\tau_{NR0}} e^{-\frac{\Delta E}{kT}}. \quad (5)$$

To probe the strength of nonradiative transitions compared to radiative transitions, one can also use the temperature-dependent fluorescence quantum efficiency ($\eta_Q(T)$), as the ratio of ions making a radiative transition via the following definition:

$$\eta_Q(T) = \frac{\tau_F(T)}{\tau_R(T)}. \quad (6)$$

The gold color dashed curves in Fig. 4 represent the calculated best-fit curves to the temperature dependence of the radiative lifetime $\tau_R(T)$ for each crystal using Eq. (3). The black solid curves represent the overall fit to the measured fluorescence lifetime data using Eq. (5). The respective fluorescence lifetime fits for each crystal were found by regression analysis where Root Mean Squared Error (RMSE) is employed as the performance indicator of the model. The corresponding fit constants (for lowest RMSE) of best-fit curves for each crystal are summarized in Table 1. Lastly, the solid green curve represents the estimated variation of fluorescence quantum efficiency with temperature $\eta_{RE}(T)$ for each material (Eq. (6)). Note that the previous studies with

Cr:Colquiriites reported a fluorescence quantum efficiency of unity ($\eta_Q \sim 1$) at low temperatures, thus $\tau_f \approx \tau_R$ for $T \ll 300$ K [53,55,56], and hence in our analysis, the fluorescence quantum efficiencies are assumed to be 1 at cryogenic temperatures.

Table 1. Empirical fit parameters to the measured fluorescence lifetime data of Cr:Colquiriites. see Eq. (3)–(6).

	Cr:LiCAF	Cr:LiSAF	Cr:LiSGaF
τ_{R0} (μ s)	195.6 ± 0.3	62.6 ± 0.3	81.7 ± 0.3
α (10^{-6} K $^{-1}$)	447 ± 2	-445 ± 3	-293 ± 3
τ_{NR0} (ps)	0.11 ± 0.05	2.4 ± 0.5	3.3 ± 0.5
ΔE (cm $^{-1}$)	8235 ± 50	4200 ± 50	4325 ± 50
$T_{1/2}$ (K)	563 ± 5	350 ± 5	363 ± 5

We see from Fig. 4 that, in the low-temperature range, for Cr:LiCAF, the measured lifetime monotonically decreases from 193 μ s at 78 K to 170 μ s at 300 K, and later to 164 μ s at 400 K. A similar trend in the radiative lifetime of Cr:LiCAF was already reported by Payne *et al.*: fluorescence lifetime decreased from around 200 μ s at 20 K to 175 μ s at 300 K [57]. The slight increase in lifetime at low temperatures is reported to be due to an additional small vibronic contribution to the oscillator strength at room temperature [47] (typical behavior under a centrosymmetric environment without non-radiative decay [58]). In comparison with Cr:LiCAF, at low temperatures, a monotonic increase of lifetime is observed for Cr:LiSAF (from 66 μ s at 78 K to 89 μ s at 255 K) and Cr:LiSGaF (from 85 μ s at 78 K to 89 μ s at 265 K) as the respective crystals are heated towards room temperature. Data reported in [7,53] show a similar behavior of fluorescence lifetime in Cr:LiSAF over cryogenic temperatures which is attributed to the slight rearrangement of the LiSAF lattice since the fluorescence lifetime of Cr $^{3+}$ is sensitive to the exact positions of the surrounding ions [53]. In addition, Kuze *et al.* showed that for decreasing temperatures in Cr:LiSAF, the tendency of even-parity strain mode of AlF $_6$ and CrF $_6$ octahedra towards more positive values could act as complementary to the decreased vibrational motion, thus resulting in an overall slight decrease of measured lifetime over this range [59]. Similar arguments may be made for Cr:LiSGaF due to its similar structural properties with Cr:LiSAF. Overall, the empirical fit parameters given in Table 1 could be used to obtain an estimate for the temperature dependence of radiative lifetime in each Cr:Colquiriite crystal. In this way, a convenient expression could be obtained for extrapolation of the radiative lifetime $\tau_R(T)$ to higher temperatures which we have later used in the calculation of emission cross-section curves using Eqs. (1) and (2).

The variation of the fluorescence lifetimes above room temperature (see Fig. 4) shows that Cr:LiCAF is superior in terms of resistance to thermal quenching. This is linked to the empirical fit parameters: ΔE and τ_{NR0} , which is shown in Table 1. The activation energy for thermal quenching ΔE for Cr:LiCaF is estimated to be 8235 cm $^{-1}$, which is considerably higher than the values estimated for Cr:LiSAF (4200 cm $^{-1}$) and Cr:LiSGaF (4325 cm $^{-1}$). Due to the higher activation energy, thermal quenching of fluorescence lifetime in Cr:LiCAF starts at much higher temperatures compared to Cr:LiSAF and Cr:LiSGaF. Another way to quantify this is by comparing the critical temperature for thermal quenching: $T_{1/2}$. This temperature is defined as the temperature at which the rate of radiative and nonradiated transitions are equal to each other (or the temperature at which the fluorescence lifetime drops to half of the radiative lifetime value). We have calculated $T_{1/2}$ as 563 K (290 °C), 350 K (77 °C), and 363 K (90 °C) for Cr:LiCAF, Cr:LiSAF and Cr:LiSGaF, respectively. The fit parameters, τ_{R0} , τ_{NR0} , ΔE , and $T_{1/2}$ are in fairly good agreement with the literature (note that the earlier studies assumed a constant radiative lifetime resulting in some difference in the fit parameters) [33,53,60].

We conclude this section with Table 2, which tabulates the measured and estimated radiative and fluorescence lifetimes for Cr:Colquiriites at selected temperatures. A comparison with the values reported in the literature is also provided [7,14,53,57,61].

Table 2. Representative values of measured and/or calculated radiative lifetimes, fluorescence lifetimes, and fluorescence quantum efficiencies for Cr:Colquiriites at selected temperatures. Earlier reports from the literature are also included for comparison.

Material	Temperature (K)	τ_R (T) (μ s)	τ_F (T) (μ s)	$\eta_{RE}(T)$ (%)
Cr:LiCAF	78	193	193, 190 [56]	100
	200	179	178	~100
	300	171	170, 175 [60]	~100
	400	164	164	~100
Cr:LiSAF	78	65	65, 64 [56]	100
	200	68	68	100
	300	71	68, 67 [7], 70 [53]	~96
	400	75	8	~10
Cr:LiSGaF	78	85	85	100
	200	86	86	100
	300	89	87, 88 [14]	~98
	400	92	16	~17

3.2. Emission cross-section measurement results

Figure 5 summarizes the emission cross-section measurement results for Cr:LiCAF. In Fig. 5 (a), we show the measured σ_e for both E \perp c and E \parallel c polarizations at 78 K and room temperature (300 K) between 650 nm and 1050 nm. In Fig. 5 (b), we show the same results in normalized logarithmic units in a broader spectral range (550–1150 nm) for better visibility at the shoulders of the spectrum. The emission spectra measured for both polarizations at room temperature are typical of the $^4T_2 \rightarrow ^4A_2$ transition. The peak of the $^4T_2 \rightarrow ^4A_2$ emission at room temperature is centered at 772 nm and has a cross-section of around $1.3 \times 10^{-20} \text{ cm}^2$ and $0.9 \times 10^{-20} \text{ cm}^2$ for E \parallel c and E \perp c polarizations, respectively. These values match the initial results of Payne *et al.* quite well [13]. Note that the emission of Cr:LiCAF at room temperature covers the whole 600–1150 nm region (Fig. 5 (b)), whereas the demonstrated tuning range is 720–887 nm [12,62]. The laser tuning range of Cr:LiCAF is limited by self-absorption losses in the short wavelength range and by ESA in the long wavelength range [12,62], and hence the emission spectrum shown in Fig. 5 does not directly reflect the gain spectrum.

At 78 K, the measured emission spectrum is structured with local peaks seen in Fig. 5 (a). The vibrational assignments of these peaks are reported at 20 K in [61]. With decreasing temperatures, a shift of the emission spectrum towards shorter wavelengths and a narrowing of the emission bandwidth are also visible. The peak emission wavelength shifts from 772 nm at 300 K to 743 nm at 78 K, and the peak σ_e values for E \parallel c and E \perp c polarizations at 78 K become $1.6 \times 10^{-20} \text{ cm}^2$ and $0.8 \times 10^{-20} \text{ cm}^2$, respectively. As expected, with decreasing temperatures, we see an increase of emission strength in E \parallel c polarization, but interestingly a decrease of emission strength in E \perp c polarization. The literature provides only the cryogenic σ_e data of Cr:LiCAF for unpolarized light in normalized units [61], so we cannot perform a comparison with the literature for the 78 K data measured in this study.

Figure 5 (c) shows the measured variation of peak σ_e value in the 78–618 K range (for this graph, the data shown in Fig. 3 are analyzed with a simple Matlab code, and the relevant

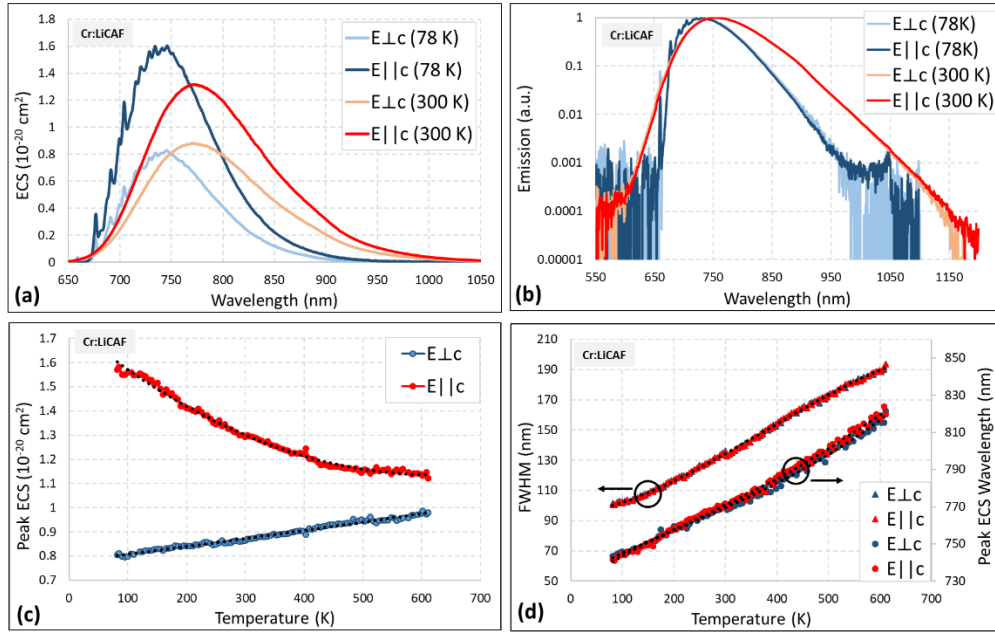


Fig. 5. Measured temperature-dependent characteristics of σ_e in E \perp c and E \parallel c polarizations of Cr:LiCAF: (a) σ_e at 77 K and 300 K, (b) Normalized emission spectra at 78 K and 300 K in logarithmic scale, (c) Variation of the peak value of σ_e , (d) peak emission wavelength and emission FWHM with temperature in the 78-618 K range.

information is extracted). Note that the ratio of peak emission cross-sections in E \parallel c and E \perp c polarizations increase from ≈ 1.15 at 600 K to ≈ 1.5 at 300 K, and to ≈ 2 at 78 K. Hence, cooling of Cr:LiCAF crystal enhances E \parallel c emission, which is favorable for laser action. Finally, in Fig. 5 (d), we present the measured variation of emission bandwidth and peak emission wavelength for both polarizations. Here, as expected, with increasing temperature, the emission spectra get broader and shift to longer wavelengths. The FWHM of emission for both polarizations increases from around 95 nm to 195 nm with increasing temperature (78 K \rightarrow 618 K) whereas the peak emission wavelength for both polarizations shifts from 743 nm to 823 nm.

For Cr:LiSAF, the emission cross-section measured in this work at room temperature and at 78 K is shown in Fig. 6 (a) and (b). The peak of the $^4T_2 \rightarrow ^4A_2$ emission at room temperature is measured at 855 nm and has a cross-section of around $4.5 \times 10^{-20} \text{ cm}^2$ and $1.45 \times 10^{-20} \text{ cm}^2$ for E \parallel c and E \perp c polarizations, respectively. The measured peak emission wavelength (855 nm) is in good agreement with the free-running laser wavelengths reported in the literature (835-860 nm [35,63]). Note also that the emission spectrum has a rather flat structure around 850 nm, which helps to minimize gain narrowing effects. The emission of Cr:LiSAF at room temperature also covers the whole 650-1350 nm region (Fig. 6 (b)), whereas the demonstrated tuning range of Cr:LiSAF so far is limited to 770-1110 nm range [35], which is again limited by self-absorption losses in the short wavelength range and the presence of ESA on the long wavelength side [48]. As a side point, the values of peak emission cross-section measured for Cr:LiSAF in this work are slightly (8-10%) lower than that reported by Payne *et al.* ($4.8 \times 10^{-20} \text{ cm}^2$ and $1.6 \times 10^{-20} \text{ cm}^2$) [7]. This is in part due to the slightly longer radiative lifetime used in this study (67 μs in [7] versus 71 μs at 300 K in this work). Moreover, our emission spectra are recorded for a wider spectral range than earlier studies, which could also contribute to the observed difference (the integrated spectral intensity is larger in Eqs. (1)–(2), which reduces the peak σ_e value).

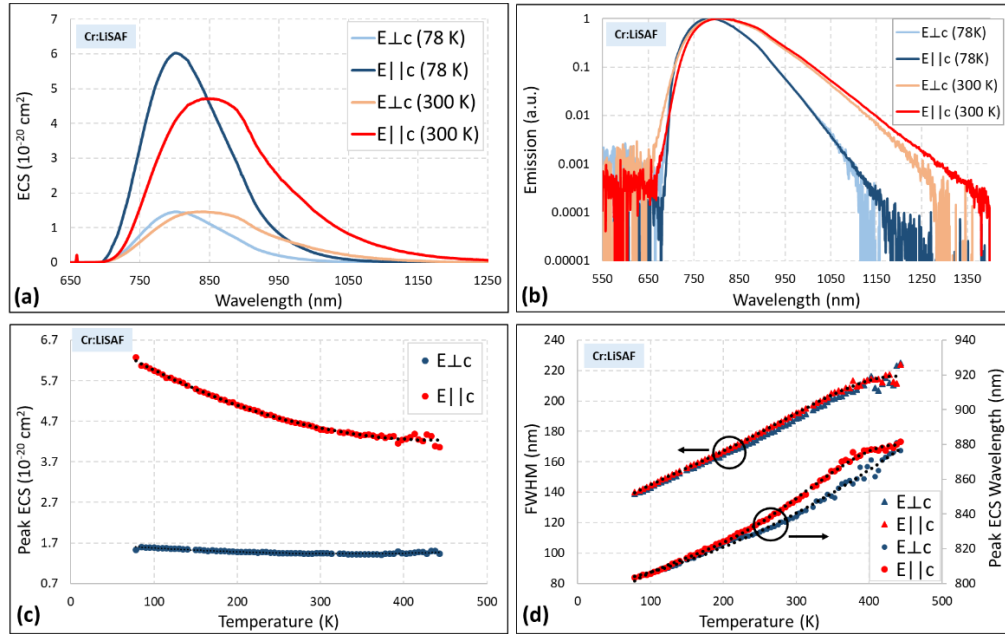


Fig. 6. Measured temperature-dependent characteristics of σ_e in E \perp c and E \parallel c polarizations of Cr:LiSAF: (a) σ_e at 77 K and 300 K, (b) Normalized emission spectra at 78 K and 300 K in logarithmic units, (c) Variation of the peak value of σ_e , (d) peak emission wavelength and emission FWHM with temperature in the 78–443 K range.

When we look at the emission spectra at 78 K, we see that the underlying structure of emission is washed out in Cr:LiSAF, consistent with the report of unpolarized emission measurement at 20 K [61]. When the crystal is cooled to 78 K, the peak σ_e for E \parallel c-polarization increases to $6.2 \times 10^{-20} \text{ cm}^2$, whereas that for E \perp c polarization only slightly increases to $1.6 \times 10^{-20} \text{ cm}^2$. For both polarizations, the peak emission wavelength shifts to $\sim 803 \text{ nm}$. Similar to Cr:LiCAF, since earlier cryogenic emission cross-section data for Cr:LiSAF in the literature is only given for unpolarized light and in normalized units [61], a comparison with literature is not possible for cryogenic emission data.

The measured temperature dependence of the peak σ_e value in Cr:LiSAF in the 78–443 K range for both polarizations is illustrated in Fig. 6 (c). We see a decrease of the σ_e strength in E \parallel c polarization from $6.20 \times 10^{-20} \text{ cm}^2$ at 78 K to $4.05 \times 10^{-20} \text{ cm}^2$ at 443 K with increasing temperature. For the E \perp c polarization, we see a very slight decrease from $1.6 \times 10^{-20} \text{ cm}^2$ at 78 K to $1.5 \times 10^{-20} \text{ cm}^2$ at 443 K. As a result, the ratio of peak emission cross sections in E \parallel c and E \perp c polarizations increases from ≈ 2.7 at 443 K to ≈ 3.1 at 300 K, and to ≈ 3.9 at 78 K. Hence, compared with Cr:LiCAF, we see a much stronger E \parallel c to E \perp c emission ratio in Cr:LiSAF, which provides a greater advantage while implementing E \parallel c configuration for lasing. The temperature-dependence of emission width and peak emission wavelength for Cr:LiSAF is shown in Fig. 6 (d). Similar to the behavior observed with Cr:LiCAF, while heating from 78 K up to 443 K, the FWHM increases linearly from 140 nm to 223 nm, whereas the peak σ_e wavelength for both polarizations shifts from 800 nm at 78 K to 881 nm at 443 K.

Figures 7 (a)–(b) show the polarized emission spectrum of Cr:LiSGaF. For Cr:LiSGaF, the peak of the ${}^4T_2 \rightarrow {}^4A_2$ emission at room temperature is measured at 826 nm and has a cross-section of $3.1 \times 10^{-20} \text{ cm}^2$ and $1.6 \times 10^{-20} \text{ cm}^2$ for E \parallel c and E \perp c polarizations, respectively. Note that, Cr:LiSGaF room-temperature emission peak (826 nm) resides in between Cr:LiCAF (772 nm)

and Cr:LiSAF (855 nm). Moreover, the peak σ_e for E||c polarization ($3.1 \times 10^{-20} \text{ cm}^2$) is also in between the value of Cr:LiCAF ($1.3 \times 10^{-20} \text{ cm}^2$) and Cr:LiSAF ($4.5 \times 10^{-20} \text{ cm}^2$). The measured values of peak σ_e for Cr:LiSGaF are slightly ($\sim 5\%$) lower than that reported earlier [14]. For Cr:LiSGaF, we believe this difference is probably due to the more sensitive measurement of fluorescence signal for a wider detection range in this work. The room-temperature emission spectra of Cr:LiSGaF have a FWHM of 169 nm, and cover from 650 nm to 1250 nm (Fig. 7 (b)). The demonstrated tuning range of Cr:LiSGaF (777-977 nm [63]) is again quite narrow concerning the measured emission spectral width. We believe the tuning range of Cr:LiSGaF laser might be further extended on the long wavelength side, as the tuning limits of this material have not been thoroughly investigated yet. Similar to Cr:LiSAF, the emission data of Cr:LiSGaF at 78 K do not show sub-structure superimposed on the emission spectrum. This is consistent with the unpolarized Cr:LiSGaF emission spectrum at 24 K reported in [14]. In the case of Cr:LiSGaF, when the crystal is cooled to 78 K, the peak emission cross section of E||c and E \perp c polarizations increases to $4.0 \times 10^{-20} \text{ cm}^2$ and $1.7 \times 10^{-20} \text{ cm}^2$, respectively.

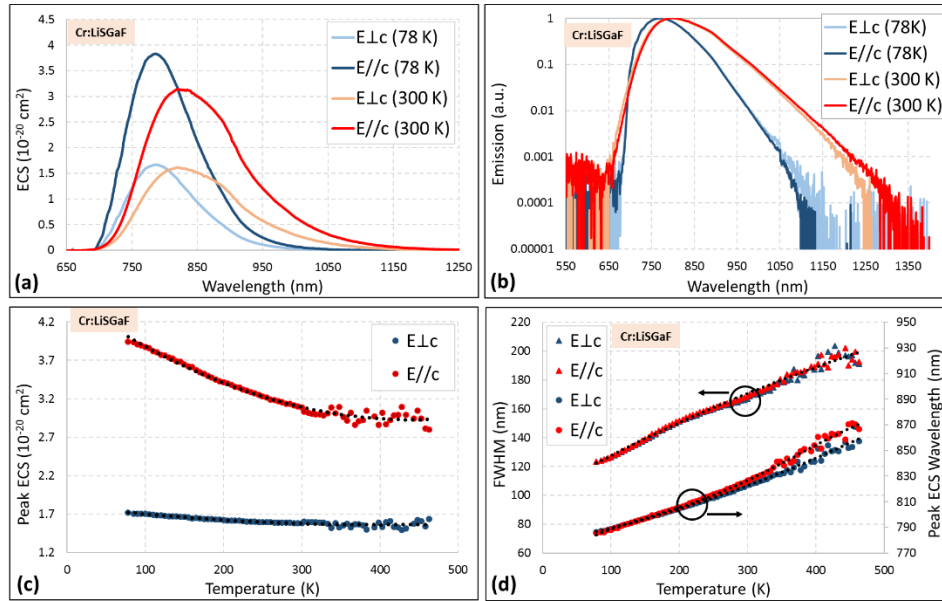


Fig. 7. Measured temperature-dependent characteristics of σ_e in E \perp c and E||c polarizations of Cr:LiSGaF: (a) σ_e at 77 K and 300 K, (b) Normalized emission spectra at 78 K and 300 K in logarithmic units, (c) Variation of the peak value of σ_e , (d) peak emission wavelength and emission FWHM with temperature in the 78-463 K range.

The measured temperature variation of Cr:LiSGaF peak σ_e in the 78-463 K range is shown in Fig. 7 (c). The σ_e strength in E||c polarization decreases from $4.0 \times 10^{-20} \text{ cm}^2$ at 78 K to $2.8 \times 10^{-20} \text{ cm}^2$ at 463 K. For the E \perp c polarization, we see a very slight decrease from $1.7 \times 10^{-20} \text{ cm}^2$ at 78 K to $1.5 \times 10^{-20} \text{ cm}^2$ at 463 K. The ratio of peak σ_e for two polarization increases from ≈ 1.85 at 463 K to ≈ 1.95 at 300 K, and to ≈ 2.3 at 78 K. Above 310 K, this trend in σ_e strength data is relatively less discernable in comparison to Cr:LiSAF due to the lower SNR caused by the shorter Cr:LiSGaF sample used during experiments. From Fig. 7 (d), in heating from 78 K to 463 K, the FWHM in both axes is seen to widen from 123 nm to 200 nm whereas the peak emission wavelength makes a shift from 786 nm to 867 nm.

In closing this section, we would like to provide empirical fit equations for the temperature dependence of important σ_e parameters of Cr:Colquiriites. We adopted the forth-order polynomial

functions with respective fit constants (a_{0-4} , b_{0-2} , c_{0-4}) resulting in minimum Root Mean Squared Error for fitting as follows:

$$\lambda_p(T) = a_0 + a_1T + a_2T^2 + a_3T^3 + a_4T^4, \quad (7)$$

$$\sigma_e(\lambda_p, T) = b_0 + b_1T + b_2T^2, \quad (8)$$

$$\Delta\lambda_e(T) = c_0 + c_1T + c_2T^2 + c_3T^3 + c_4T^4 \quad (9)$$

Above, $\lambda_p(T)$ is the peak emission wavelength, $\sigma_e(\lambda_p, T)$ is the σ_e at the peak emission wavelength, and $\Delta\lambda_e(T)$ is the full-width at half-maximum of the measured emission spectra. The respective best-fit results are shown in Figs. 5–7 by black dashed lines and the relevant best-fit parameters for all three crystals are given in Tables 3–5. Furthermore, for easier access, Table 6 tabulates measured/fit values for the peak emission wavelength, peak σ_e , and emission FWHM for all crystals, for the E||c polarization at selected temperatures.

Table 3. Best fit values of the temperature coefficients in Eq. (7) for the estimation of peak emission wavelength (in nm) in E⊥c and E||c polarizations of Cr:Colquiriites.

	Axis	$a_4(K^{-4})$	$a_3(K^{-3})$	$a_2(K^{-2})$	$a_1(K^{-1})$	a_0
Cr:LiCAF	E c	-3.6×10^{-10}	6.86×10^{-7}	-3.75×10^{-4}	2.13×10^{-1}	725.3
	E⊥c	-	1.8×10^{-7}	-1.1×10^{-4}	1.43×10^{-1}	731.6
Cr:LiSAF	E c	-1.43×10^{-8}	1.32×10^{-5}	-3.95×10^{-3}	6.5×10^{-1}	769.1
	E⊥c	-	7.3×10^{-7}	-3.1×10^{-4}	2×10^{-1}	788.25
Cr:LiSGaF	E c	-5.28×10^{-9}	5.61×10^{-6}	-1.84×10^{-3}	4.06×10^{-1}	761.4
	E⊥c	-	-	1.64×10^{-4}	1×10^{-1}	777.7

Table 4. Best fit values of the temperature coefficients in Eq. (8) for the estimation of peak σ_e value (in 10^{-20} cm^2) in E⊥c and E||c polarizations of Cr:Colquiriites.

	Axis	$b_2(K^{-2})$	$b_1(K^{-1})$	b_0
Cr:LiCAF	E c	1.62×10^{-6}	-2×10^{-3}	1.755
	E⊥c	-	3.35×10^{-4}	0.773
Cr:LiSAF	E c	1.47×10^{-5}	-1.3×10^{-2}	7.127
	E⊥c	2.65×10^{-6}	-1.76×10^{-3}	1.726
Cr:LiSGaF	E c	8.17×10^{-6}	-7.22×10^{-3}	4.52
	E⊥c	1.54×10^{-6}	-1.24×10^{-3}	1.81

Table 5. Best fit values of the temperature coefficients in Eq. (9) for the estimation of emission spectrum width (FWHM) (in nm) in Cr:Colquiriites. The emission width is found to be independent of polarization.

	$c_4(K^{-4})$	$c_3(K^{-3})$	$c_2(K^{-2})$	$c_1(K^{-1})$	c_0
Cr:LiCAF	-	-3.6×10^{-7}	4.1×10^{-4}	4.5×10^{-2}	93.75
Cr:LiSAF	-7.1×10^{-9}	6.1×10^{-6}	-1.76×10^{-3}	4.3×10^{-1}	114
Cr:LiSGaF		6.14×10^{-8}	-1.65×10^{-4}	2.74×10^{-1}	101.7

Table 6. Representative values of measured/calculated peak emission wavelength, peak σ_e , and emission bandwidth for Cr:Colquiriites at selected temperatures. Earlier reports from the literature are also included for comparison.

Material	Temperature (K)	$\lambda_p(T)$ for E c (nm)	$\sigma_e(\lambda_p, T)$ for E c (10^{-20} cm ²)	$FWHM(T)$ (nm)
Cr:LiCAF	100	744	1.56	102
	200	759	1.41	117
	300	772	1.29, 1.3 [13]	135
	400	786	1.23	155
Cr:LiSAF	100	807	5.93	144
	200	823	5.07	168
	300	855	4.48, 4.8 [7]	189
	385	875	4.43	206
Cr:LiSGaF	100	788	3.87	127
	200	806	3.41	152
	300	826	3.09, 3.3 [14]	169
	400	860	3.01	191

4. Conclusion

We have investigated the temperature dependence of the fluorescence lifetime and polarized emission strength for Cr:LiCAF, Cr:LiSAF, and Cr:LiSGaF crystals over the 78–618 K range. To the best of our knowledge, this study presents the first detailed experimental cryogenic spectroscopy data for Cr:Colquiriites. We observed a temperature-dependent radiative lifetime in all three crystals when cooling in the range of 300–78 K: 1.15-fold increase in Cr:LiCAF (from 170 μ s to 195 μ s), 1.08-fold decrease in Cr:LiSAF (from 71 μ s to 66 μ s), and a slight 1.04-fold decrease in Cr:LiSGaF (from 88 μ s to 85 μ s). We have also seen that, by cooling to cryogenic temperatures, the peak σ_e value in E||c polarization improves \sim 1.2-fold in Cr:LiCAF, \sim 1.4-fold in Cr:LiSAF, and \sim 1.3-fold in Cr:LiSGaF. The emission bandwidth (FWHM) at 78 K is measured as 100 nm in Cr:LiCAF, 140 nm in Cr:LiSAF and 123 nm in Cr:LiSGaF (narrows down 1.25-fold in Cr:LiCAF, 1.28-fold in Cr:LiSAF, and 1.27-fold in Cr:LiSGaF). These bandwidths at cryogenic temperatures are quite sufficient for the generation/amplification of sub-50-fs level pulses.

The improvement in emission cross-section at cryogenic temperatures is rather moderate (1.2 to 1.4 fold) in Cr:Colquiriites. On the other hand, at cryogenic operation, one is further away from temperatures where nonradiative transitions become significant, which may in turn enable the application of at least 2–3-fold higher pump powers compared to room-temperature systems. Furthermore, several-fold improvement in the thermal conductivity of materials is expected by cooling to cryogenic temperatures [45]. Hence, we believe that, as in the case of Yb-based materials, an order of magnitude improvement in obtainable output powers is feasible in cryogenically cooled Cr:Colquiriite laser/amplifier systems. This study solely focusing on spectroscopic aspects is the first step to fully reveal the potential of Cr:Colquiriites lasers at cryogenic temperatures. Further work to understand the temperature dependence of thermo-mechanical and thermo-optical parameters such as thermal conductivity, thermal expansion coefficient, refractive index, etc. is required for accurate modeling of cryogenic Cr:Colquiriite lasers.

Funding. Türkiye Bilimsel ve Teknolojik Araştırma Kurumu (1059B142100385, 119E264).

Disclosures. The authors declare no conflicts of interest.

Data availability. Data underlying the results presented in this paper are not publicly available at this time but may be obtained from the authors upon reasonable request.

References

1. A. Sennaroglu and Y. Morova, "Divalent (Cr^{2+}), trivalent (Cr^{3+}), and tetravalent (Cr^{4+}) chromium ion-doped tunable solid-state lasers operating in the near and mid-infrared spectral regions," *Appl. Phys. B* **128**(1), 1–25 (2022).
2. I. T. Sorokina, " Cr^{2+} -doped II-VI materials for lasers and nonlinear optics," *Opt. Mater.* **26**(4), 395–412 (2004).
3. S. B. Mirov, I. S. Moskalev, S. Vasilyev, V. Smolski, V. V. Fedorov, D. Martyshev, J. Peppers, M. Mirov, A. Dergachev, and V. Gapontsev, "Frontiers of mid-IR lasers based on transition metal doped chalcogenides," *IEEE J. Sel. Top. Quantum Electron.* **24**(5), 1 (2018).
4. U. Demirbas, "Cr:Colquirite Lasers: Current status and challenges for further progress," *Prog. Quantum Electron.* **68**, 100227 (2019).
5. A. Sennaroglu, "Broadly tunable Cr^{4+} -doped solid-state lasers in the near infrared and visible," *Prog. Quantum Electron.* **26**(6), 287–352 (2002).
6. T. H. Maiman, "Stimulated Optical Radiation in Ruby," *Nature* **187**(4736), 493–494 (1960).
7. S. A. Payne, L. L. Chase, L. K. Smith, W. L. Kway, and H. W. Newkirk, "Laser performance of $\text{LiSrAlF}_6\text{:Cr}^{3+}$," *J. Appl. Phys.* **66**(3), 1051–1056 (1989).
8. M. Shand and S. Lai, "CW laser pumped emerald laser," *IEEE J. Quantum Electron.* **20**(2), 105–108 (1984).
9. S. T. Lai, "Highly efficient emerald laser," *J. Opt. Soc. Am. B* **4**(8), 1286–1290 (1987).
10. J. C. Walling, H. P. Jenssen, R. C. Morris, E. W. O'Dell, and O. G. Peterson, "Tunable-laser performance in $\text{BeAl}_2\text{O}_4\text{:Cr}^{3+}$," *Opt. Lett.* **4**(6), 182–183 (1979).
11. S. T. Lai and M. L. Shand, "High-Efficiency Cw Laser-Pumped Tunable Alexandrite Laser," *J. Appl. Phys.* **54**(10), 5642–5644 (1983).
12. S. A. Payne, L. L. Chase, H. W. Newkirk, L. K. Smith, and W. F. Krupke, " $\text{LiCaAlF}_6\text{:Cr}^{3+}$: a promising new solid-state laser material," *IEEE J. Quantum Electron.* **24**(11), 2243–2252 (1988).
13. S. A. Payne, L. L. Chase, L. K. Smith, and B. H. T. Chai, "Flashlamp-pumped laser performance of $\text{LiCaAlF}_6\text{:Cr}^{3+}$," *Opt. Quantum Electron.* **22**(S1), S259–S268 (1990).
14. L. K. Smith, S. A. Payne, W. L. Kway, L. L. Chase, and B. H. T. Chai, "Investigation of the laser properties of $\text{Cr}^{3+}\text{:LiSrGaF}_6$," *IEEE J. Quantum Electron.* **28**(11), 2612–2618 (1992).
15. E. Sorokin, "Solid-state materials for few-cycle pulse generation and amplification," in *Few-Cycle Laser Pulse Generation and Its Applications*, F. X. Kärtner, ed. (Springer-Verlag, 2004), **95**, pp. 3–71.
16. M. Fibrich, J. Šulc, D. Vyhlídal, H. Jelínková, and M. Čech, "Alexandrite spectroscopic and laser characteristic investigation within a 78–400 K temperature range," *Laser Phys.* **27**(11), 115801 (2017).
17. E. Sorokin, I. T. Sorokina, and E. Wintner, "Diode-pumped ultra-short-pulse solid-state lasers," *Appl. Phys. B* **72**(1), 3–14 (2001).
18. C. T. A. Brown, M. A. Cataluna, A. A. Lagatsky, E. U. Rafailov, M. B. Agate, C. G. Leburn, and W. Sibbett, "Compact laser-diode-based femtosecond sources," *New J. Phys.* **6**, 1–21 (2004).
19. P. Wagenblast, U. Morgner, F. Grawert, V. Scheuer, G. Angelow, M. J. Lederer, and F. X. Kärtner, "Generation of sub-10-fs pulses from a Kerr-lens modelocked $\text{Cr}^{3+}\text{:LiCAF}$ laser oscillator using third order dispersion compensating double chirped mirrors," *Opt. Lett.* **27**(19), 1726–1729 (2002).
20. F. Grawert, F. X. Kärtner, G. Angelow, M. J. Lederer, P. C. Wagenblast, T. R. Schibli, U. Morgner, V. Scheuer, F. Grawert, T. R. Schibli, F. X. Kärtner, V. Scheuer, G. Angelow, and M. J. Lederer, "Generation of sub-10-fs pulses from a Kerr-lens mode-locked $\text{Cr}^{3+}\text{:LiCAF}$ laser oscillator by use of third-order dispersion-compensating double-chirped mirrors," *Opt. Lett.* **27**(19), 1726 (2002).
21. I. T. Sorokina, E. Sorokin, E. Wintner, A. Cassanho, H. P. Jenssen, and R. Szpöcs, "14-fs pulse generation in Kerr-lens mode-locked prismless $\text{Cr}\text{:LiSGaF}$ and $\text{Cr}\text{:LiSAF}$ lasers: observation of pulse self-frequency shift," *Opt. Lett.* **22**(22), 1716 (1997).
22. S. Uemura, K. Torizuka, and S. Uemura, "Generation of 12-fs pulses from a diode-pumped Kerr-lens mode-locked $\text{Cr}\text{:LiSAF}$ laser," *Opt. Lett.* **24**(11), 780 (1999).
23. R. Ell, U. Morgner, F. X. Kärtner, J. G. Fujimoto, E. P. Ippen, V. Scheuer, G. Angelow, T. Tschudi, M. J. Lederer, A. Boiko, and B. Luther-Davies, "Generation of 5-fs pulses and octave-spanning spectra directly from a Ti:sapphire laser," *Opt. Lett.* **26**(6), 373–375 (2001).
24. D. Klimm, G. Lacayo, and P. Reiche, "Growth of $\text{Cr}\text{:LiCaAlF}_6$ and $\text{Cr}\text{:LiSrAlF}_6$ by the Czochralski method," *J. Cryst. Growth* **210**(4), 683–693 (2000).
25. V. Kubecek, R. Quintero-Torres, and J. C. Diels, "Ultralow-pump-threshold laser diode pumped $\text{Cr}\text{:LiSAF}$ laser," *Adv. Lasers Syst.* **5137**, 43–47 (2002).
26. D. Li, U. Demirbas, A. Benedick, A. Sennaroglu, J. G. Fujimoto, and F. X. Kärtner, "Attosecond timing jitter pulse trains from semiconductor saturable absorber mode-locked $\text{Cr}\text{:LiSAF}$ lasers," *Opt. Express* **20**(21), 23422 (2012).
27. A. Isemann and C. Fallnich, "High-power Colquirite lasers with high slope efficiencies pumped by broad-area laser diodes," *Opt. Express* **11**(3), 259 (2003).
28. S. Uemura and K. Miyazaki, "Thermal characteristics of a continuous-wave $\text{Cr}\text{:LiSAF}$ laser," *Jpn. J. Appl. Phys.* **36**(7A), 4312–4315 (1997).
29. U. Demirbas, "Power scaling potential of continuous-wave $\text{Cr}\text{:LiSAF}$ and $\text{Cr}\text{:LiCAF}$ lasers in thin-disk geometry," *Appl. Opt.* **57**(35), 10207 (2018).
30. B. W. Woods, S. A. Payne, J. E. Marion, R. S. Hughes, and L. E. Davis, "Thermomechanical and thermo-optic properties of the $\text{LiCaAlF}_6\text{-Cr}^{3+}$ laser material," *J. Opt. Soc. Am. B* **8**(5), 970–977 (1991).

31. U. Demirbas and D. A. E. Acar, "Continuous-wave, quasi-continuous-wave, gain-switched, and femtosecond burst-mode operation of multi-mode diode-pumped Cr:LiSAF lasers," *J. Opt. Soc. Am. B* **33**(10), 2105 (2016).
32. J. M. Eichenholz and M. Richardson, "Measurement of thermal lensing in Cr³⁺-doped colquiriites," *IEEE J. Quantum Electron.* **34**(5), 910–919 (1998).
33. A. Dergachev, J. H. Flint, Y. Isyanova, B. Pati, E. V. Slobodtchikov, K. F. Wall, and P. F. Moulton, "Review of multipass slab laser systems," *IEEE J. Sel. Top. Quantum Electron.* **13**(3), 647–660 (2007).
34. D. Kopf, K. J. Weingarten, G. Zhang, M. Moser, M. A. Emanuel, R. J. Beach, J. A. Skidmore, and U. Keller, "High-average-power diode-pumped femtosecond Cr:LiSAF lasers," *Appl. Phys. B* **65**(2), 235–243 (1997).
35. U. Demirbas and I. Baali, "Power and efficiency scaling of diode pumped Cr:LiSAF lasers: 770–1110 nm tuning range and frequency doubling to 387–463 nm," *Opt. Lett.* **40**(20), 4615–4618 (2015).
36. U. Demirbas, I. Baali, D. A. E. Acar, and A. Leitenstorfer, "Diode-pumped continuous-wave and femtosecond Cr:LiCAF lasers with high average power in the near infrared, visible and near ultraviolet," *Opt. Express* **23**(7), 8901 (2015).
37. R. E. Samad, S. L. Baldochi, G. E. C. Nogueira, and N. D. Vieira, "30 W Cr : LiSrAlF₆ flashlamp-pumped pulsed laser," *Opt. Lett.* **32**(1), 50–52 (2007).
38. D. E. Klimek and A. Mandl, "Power scaling of a flashlamp-pumped Cr:LiSAF thin-slab zig-zag laser," *IEEE J. Quantum Electron.* **38**(12), 1607–1613 (2002).
39. D. Rand, D. Miller, D. J. Ripin, and T. Y. Fan, "Cryogenic Yb³⁺-doped materials for pulsed solid-state laser applications [Invited]," *Opt. Mater. Express* **1**(3), 434–450 (2011).
40. L. E. Zapata, M. Pergament, M. Schust, S. Reuter, J. Thesinga, C. Zapata, M. Kellert, U. Demirbas, A.-L. Calendron, Y. Liu, and F. X. Kärtner, "One-joule 500-Hz cryogenic Yb:YAG laser driver of composite thin-disk design," *Opt. Lett.* **47**(24), 6385–6388 (2022).
41. T. Y. Fan, D. J. Ripin, R. L. Aggarwal, J. R. Ochoa, B. Chann, M. Tilleman, and J. Spitzberg, "Cryogenic Yb³⁺-doped solid-state lasers," *IEEE J. Select. Topics Quantum Electron.* **13**(3), 448–459 (2007).
42. J. Kawanaka, S. Tokita, H. Nishioka, M. Fujita, K. Yamakawa, K. Ueda, and Y. Izawa, "Dramatically improved laser characteristics of diode-pumped Yb-doped materials at low temperature," *Laser Phys.* **15**(9), 1306–1312 (2005).
43. D. C. Brown, "The promise of cryogenic solid-state lasers," *IEEE J. Select. Topics Quantum Electron.* **11**(3), 587–599 (2005).
44. P. A. Schulz and S. R. Henion, "Liquid-nitrogen-cooled Ti:Al₂O₃ laser," *IEEE J. Quantum Electron.* **27**(4), 1039–1047 (1991).
45. D. C. Brown, S. Tornegård, J. Kolis, C. McMillen, C. Moore, L. Sanjeewa, and C. Hancock, *The Application of Cryogenic Laser Physics to the Development of High Average Power Ultra-Short Pulse Lasers* (Multidisciplinary Digital Publishing Institute, 2016), **6**(1), p. 23.
46. M. Stalder, B. H. T. Chai, and M. Bass, "Flashlamp pumped Cr:LiSrAlF₆ laser," *Appl. Phys. Lett.* **58**(3), 216–218 (1991).
47. S. A. Payne, L. L. Chase, L. J. Atherton, J. A. Caird, W. L. Kway, M. D. Shinn, R. S. Hughes, and L. K. Smith, "Properties and performance of the LiCaAlF₆:Cr³⁺ laser material," *Solid State Lasers* **1223**, 84 (1990).
48. W. R. Rapoport and M. L. Shand, "Excited state absorption and upconversion in Cr:LiSrAlF₆," *Solid State Commun.* **84**(1-2), 29–31 (1992).
49. P. F. Moulton, "Spectroscopic and laser characteristics of Ti:Al₂O₃," *J. Opt. Soc. Am. B* **3**(1), 125–133 (1986).
50. G. Huber, W. W. Krühler, W. Bludau, and H. G. Danielmeyer, "Anisotropy in the laser performance of NdP₅O₁₄," *J. Appl. Phys.* **46**(8), 3580 (1975).
51. J. Dong, M. Bass, Y. Mao, P. Deng, and F. Gan, "Dependence of the Yb³⁺ emission cross section and lifetime on temperature and concentration in yttrium aluminum garnet," *J. Opt. Soc. Am. B* **20**(9), 1975–1979 (2003).
52. L. J. Andrews, A. Lempicki, B. C. Mccollum, C. J. Giunta, R. H. Bartram, and J. F. Dolan, "Thermal Quenching of Chromium Photoluminescence in Ordered Perovskites. I. Temperature-Dependence of Spectra and Lifetimes," *Phys. Rev. B* **34**(4), 2735–2740 (1986).
53. M. Stalder, M. Bass, and B. H. T. Chai, "Thermal quenching of fluorescence in chromium-doped fluoride laser crystals," *J. Opt. Soc. Am. B* **9**(12), 2271 (1992).
54. M. A. Noginov, M. Vondrova, and B. D. Lucas, "Thermally induced optical bistability in Cr-doped colquiriite crystals," *Phys. Rev. B* **65**(3), 035112 (2002).
55. V. Pilla, S. M. Lima, T. Catunda, A. Medina, and M. L. Baesso, "Thermal lens study of the fluorescence thermal quenching in Cr³⁺-doped fluoride crystals," *4th Iberoam. Meet. Opt. 7th Lat. Am. Meet. Opt. Lasers, Their Appl.* 4419(August 2001), 138–141 (2001).
56. V. Pilla, T. Catunda, S. Marcio Lima, A. Neto Medina, M. Luciano Baesso, H. P. Jenssen, and A. Cassanho, "Thermal quenching of the fluorescence quantum efficiency in colquiriite crystals measured by thermal lens spectrometry," *J. Opt. Soc. Am. B* **21**(10), 1784 (2004).
57. S. A. Payne, L. L. Chase, H. W. Newkirk, and W. F. Krupke, "Cr³⁺-Doped Colquiriite Solid State Laser Material," Lawrence Livermore March 31, 1989.
58. R. Gvishi, E. Gonen, Y. Kalisky, and S. Rotman, "Studies of the spectroscopic behavior of Cr³⁺:LiCAF pumped by a solid-state dye laser," *Opt. Mater.* **1**, 1 (1999).

59. S. Kuze, D. Du Boulay, N. Ishizawa, N. Kodama, M. Yamaga, and B. Henderson, "Structures of LiCaAlF_6 and LiSrAlF_6 at 120 and 300 K by synchrotron X-ray single-crystal diffraction," *J. Solid State Chem.* **177**(10), 3505–3513 (2004).
60. F. Balembois, F. Druon, F. Falcoz, P. Georges, and A. Brun, "Performances of $\text{Cr}:\text{LiSrAlF}_6$ and $\text{Cr}:\text{LiSrGaF}_6$ for continuous-wave diode-pumped Q-switched operation," *Opt. Lett.* **22**(6), 387 (1997).
61. S. A. Payne, L. L. Chase, and G. D. Wilke, "Optical spectroscopy of the new laser materials, $\text{LiSrAlF}_6:\text{Cr}^{3+}$ and $\text{LiCaAlF}_6:\text{Cr}^{3+}$," *J. Lumin.* **44**(3), 167–176 (1989).
62. U. Demirbas, R. Uecker, D. Klimm, and J. Wang, "Low-cost, broadly tunable (375–433 nm & 746–887 nm) $\text{Cr}:\text{LiCAF}$ laser pumped by one single-spatial-mode diode," *Appl. Opt.* **51**(35), 8440 (2012).
63. U. Demirbas, D. Li, J. R. Birge, A. Sennaroglu, G. S. Petrich, L. A. Kolodziejski, F. X. Kärtner, and J. G. Fujimoto, "Low-cost, single-mode diode-pumped $\text{Cr}:\text{Colquiriite}$ lasers," *Opt. Express* **17**(16), 14374 (2009).